

# Functional Gaussian Process Model for Bayesian Nonparametric Analysis

Leo L. Duan

University of Cincinnati

and

Xia Wang

University of Cincinnati

and

Rhonda D. Szczesniak \*

Cincinnati Children's Hospital Medical Center

December 3, 2024

## Abstract

Gaussian process regression is a commonly used nonparametric approach in spatial statistics and functional data analyses. The parameters in the covariance function provide nice interpretation regarding the decaying pattern of the correlation. However, its computational cost obstructs its use in extremely large data or more sophisticated modeling. It is desirable to have a solution that retains the simple interpretation and estimating accuracy, without putting much restraint on the scalability or the data. For these purposes, we propose a novel Bayesian approach called the functional Gaussian process, which assumes a latent lattice process beneath the observed data. It utilizes the spectral properties and reduces the computational cost to  $N \log_2(N)$ . Specifically, this latent process enables easy sampling of the missing values, controls the error of the spectral transformation and facilitates the generalization to non-stationarity. The parameter estimates have high accuracy and the model is tolerant to data missingness and different sample sizes. For the data application in the prediction with the 30-year annual surface air temperature data, we demonstrate the estimation of three non-stationary spatial-temporal models, from a simple additive model to a non-separable space-time interactive model, using the functional Gaussian process framework. Our work allows rapid estimation and produces nicely interpretable results.

*Keywords:* Scalable Gaussian Process, Spectral Density, Missing Values, Non-Stationarity, Spatial-Temporal Model, Mixture Model

---

\*Corresponding author. Address: 3333 Burnet Ave, MLC 5041, Cincinnati, OH 45229. Phone:(513)803-0563, email: rhonda.szczesniak@cchmc.org. The authors gratefully acknowledge the Cystic Fibrosis Foundation Research and Development Program (grant number R457-CR11) for the support of this research.

# 1 Introduction

Gaussian process regression is an important nonparametric approach for analyzing continuous data. The finite-dimensional distribution of a Gaussian process has the measure of a multivariate Gaussian distribution, with which one can easily estimate the covariance structure in the data. This is probably why Gaussian process is the most commonly used model in spatial statistics. On the other hand, when the data are assumed to have a specific covariance function, it is equivalent to adding a regularization based on reproducing kernel Hilbert space [Lawrence and Jordan, 2004]. Therefore, Gaussian process regression is also often used as kernel smoother in functional data analysis. In this light, its applications cover a wide range, from computer experiment emulations [Loeppky et al., 2009] to longitudinal analyses of biomedical data [Henderson et al., 2000]. In practice, however, the likelihood evaluation of the Gaussian process involves matrix inversion or eigendecomposition, either of which requires  $O(N^3)$  operations. For a dataset of large size (usually  $N > 10^5$ ), the model fitting either takes too much time or becomes infeasible due to the large memory requirement.

To solve this issue, many methods have been proposed. They can be classified mainly in two categories. The first class involves dimension reduction and commonly approximates the matrix as a function of several reduced-rank matrices. One popular method in machine learning is to use Nyström method to approximate the top  $m$  eigenvectors in the matrix [Smola and Schölkopf, 2000, Williams and Seeger, 2001]. Another approach that emerged from spatial statistics is the use of spatial random effects [Cressie and Johannesson, 2008] to model the covariance as a quadratic transform of  $m$  predetermined basis functions, thereby simplifying the focus to estimating the  $m$  coefficients. A third approach is referred to as a predictive process [Banerjee et al., 2008], which utilizes hierarchical conditioning of the data on a subset (with size  $m$ ) of the observed locations. These methods reduce the cost of matrix inversion to  $O(m^3)$ . When the reduced rank has  $m \ll N$ , the bottleneck step is shifted to the matrix multiplication operation, which has complexity of  $O(Nm^2)$ . The strength of these models is that they allow high flexibility in the reduced-rank matrix, which in turn incorporates non-stationarity into the model. On the other hand, one may be concerned with the arbitrariness in  $m$ , whose determination involves a trade-off

between resolution and computation cost. Furthermore, interpretation becomes increasingly difficult. In other commonly used covariance functions, the parameters (for example, range) provide direct measures of how the correlation decays over distance; whereas comparatively in the aforementioned models, estimates for a matrix of size  $m \times m$  appear less straightforward.

The second class of models uses a completely different strategy to solve the issue. Rather than dimension reduction, the primary focus is on the spectral decomposition of the covariance matrix. This pioneering work was self-titled Whittle’s likelihood, as Whittle [1953] discovered a nice connection between the eigenvalues of covariance matrix and the spectral density for the time series data. Later, this likelihood was applied on two-dimensional spatial data [Fuentes, 2007] with an approximation adjustment for the irregularity in the lattice data. This school of models has several advantages. Firstly, not only the operation of matrix inversion is completely avoided, but also the matrix multiplication can be carried out with the fast Fourier transform [Cooley and Tukey, 1965], which has a complexity of  $O(N \log_2 N)$ . Secondly, the parameter estimated in Whittle’s likelihood is the same as those in ordinary covariance functions (such as squared exponential, Matérn functions, etc), thereby allowing simple interpretation. One drawback of this approach, however, is the requirement of large  $N$  and complete lattice data, for which the maximum likelihood remedies rely on the asymptotic property and may not be appropriate for a finite number of data. Another shortcoming in Whittle’s likelihood is that it lacks accommodation for non-stationarity.

In this paper, we focus on this latter class of models. In recent efforts to solve this first limitation, Stroud et al. [2014] proposed a Bayesian inference procedure and treated the incomplete lattice data as the ones with missing values. A preconditioned conjugate gradient algorithm was used to sample the missing values, for which the operation has cost of  $O(IN \log_2 N)$  and  $I$  is the iteration number needed in each time of search. For the second issue of non-stationarity, Fuentes and Smith [2001] proposed a model that uses local convolution of several stationary processes and relies on Monte Carlo integration in the estimation.

Despite our similar motivation to address these two issues, our unique contribution is

that we propose the use of a latent process that we call the functional Gaussian process, which further reduces the complexity of missing value sampling to only  $O(N \log_2 N)$  and allows a simple and straightforward extension to non-stationarity or non-Gaussianness. We investigate the properties of the spectral approach and demonstrate how various issues, such as matrix singularity, small  $N$ , incompleteness or matrix imperfection, can be solved in the Bayesian framework. In the illustrating examples and data application, we demonstrate the numerical accuracy of the proposed approach and its capability in incorporating several sophisticated models to a large dataset.

In the following sections, we first briefly review the spectral studies regarding Whittle’s likelihood and extend it to high-dimensional data. Then, we introduce the modeling structure of the functional Gaussian process and its sampling procedure, followed by the numerical studies and comparison. Next, we generalize the model to accommodate non-stationary or non-Gaussian data. Lastly, we utilize this extended framework to examine three different spatial-temporal models of a large dataset consisting of North American surface temperatures.

## 2 Spectral Studies in Finite-Dimensional Space

Since Whittle’s likelihood [Whittle, 1953] was derived in one dimension, we now extend this derivation into finite-dimensional space with  $d < \infty$ . A Gaussian process  $Z(\mathbf{s})$  with  $\mathbf{s} \in \mathbb{R}^d$  is weakly stationary when it has mean and covariance that are both shift-invariant, such that  $\mathbb{E}Z(\mathbf{s}) = \mathbb{E}Z(\mathbf{s} + \mathbf{x})$  and  $Cov(\mathbf{s}, \mathbf{t}) = Cov(\mathbf{s} + \mathbf{x}, \mathbf{t} + \mathbf{x}) = \mathbf{C}(\mathbf{s} - \mathbf{t})$  for any  $\Delta \in \mathbb{R}^d$ . If  $\int_{\mathbb{R}^d} |C(\mathbf{x})| d\mathbf{x} < \infty$ , then the spectral density function,  $g$ , can be defined as the forward Fourier transform of the covariance function:

$$g(\boldsymbol{\omega}) = \int_{\mathbb{R}^d} \exp(-i\mathbf{x}^T \boldsymbol{\omega}) C(\mathbf{x}) d\mathbf{x} \tag{1}$$

where  $i$  is the imaginary complex number  $i = \sqrt{-1}$  and  $\boldsymbol{\omega}$  is commonly known as angular frequency. By Bochner’s theorem,  $g$  is finite and positive definite if and only if  $C$  is positive definite. For any  $x_k$  in  $\mathbf{X}$ , the covariance is symmetric  $C(x_k) = C(-x_k)$ ; for any  $\omega_l$  in  $\boldsymbol{\omega}$ ,  $g(\omega_l) = g(-\omega_l)$ .

Conversely, the covariance function can be represented as the backward Fourier transform of the spectral density:

$$C(\mathbf{x}) = \frac{1}{(2\pi)^d} \int_{\mathbb{R}^d} \exp(i\mathbf{x}^T \boldsymbol{\omega}) g(\boldsymbol{\omega}) d\boldsymbol{\omega} \quad (2)$$

We can use Riemann sum to approximate the integral:

$$C_a(\mathbf{x}) = \frac{1}{N_1 N_2 \dots N_d (2\pi)^d} \sum_{j_d=1}^{N_d} \dots \sum_{j_2=1}^{N_2} \sum_{j_1=1}^{N_1} \exp(i\mathbf{x}^T \boldsymbol{\omega}_j) g(\boldsymbol{\omega}_j) \quad (3)$$

where  $\boldsymbol{\omega}_j = \{\frac{(j_1-1)}{N_1} 2\pi, \frac{(j_2-1)}{N_2} 2\pi, \dots, \frac{(j_d-1)}{N_d} 2\pi\}$  is a dense and equally spaced grid over  $[0, 2\pi)^d$ , to which the space is simplified from  $\mathbb{R}^d$  thanks to aliasing (reviewed by Fuentes [2002]). It is obvious that the equality between (2) and (3) will hold as  $N_1 N_2 \dots N_d \rightarrow \infty$ .

A lattice is defined as a regular grid such that in each dimension, the distances between two neighboring locations are the same. When the data are located on such a lattice, the increment in each dimension can be scaled to 1. For any two locations  $\mathbf{s}_1 = \{j_1, j_2, \dots, j_d\}$  and  $\mathbf{s}_2 = \{k_1, k_2, \dots, k_d\}$ , we index two row complex vectors  $\mathbf{q}_{\mathbf{s}_1}$ ,  $\mathbf{q}_{\mathbf{s}_2}$  and a real diagonal matrix  $\mathbf{D}$  by  $(m_1, m_2, \dots, m_d)$ , where  $m_k = 1, \dots, N_k$ , and define them as follows:

$$\begin{aligned} (\mathbf{q}_{\mathbf{s}_1})_{(m_1, m_2, \dots, m_d)} &= \frac{\exp(i \cdot [(j_1 - 1) \cdot \frac{m_1 - 1}{N_1} 2\pi + \dots + (j_d - 1) \cdot \frac{m_d - 1}{N_d} 2\pi])}{\sqrt{N_1 N_2 \dots N_d}} \\ (\mathbf{q}_{\mathbf{s}_2})_{(m_1, m_2, \dots, m_d)} &= \frac{\exp(i \cdot [(k_1 - 1) \cdot \frac{m_1 - 1}{N_1} 2\pi + \dots + (k_d - 1) \cdot \frac{m_d - 1}{N_d} 2\pi])}{\sqrt{N_1 N_2 \dots N_d}} \\ \mathbf{D}_{(m_1, m_2, \dots, m_d)} &= g\left(\frac{m_1 - 1}{N_1} 2\pi, \dots, \frac{m_d - 1}{N_d} 2\pi\right) / (2\pi)^d \end{aligned} \quad (4)$$

It can be verified that the matrix product  $\mathbf{q}_{\mathbf{s}_1} \mathbf{D} \mathbf{q}_{\mathbf{s}_2}^* = C_a(\mathbf{s}_1 - \mathbf{s}_2)$ , ( $(\cdot)^*$  denotes transpose conjugate), which is exactly the covariance in (3). Using  $\mathbf{q}_{(\cdot)}$ 's as the rows for the matrix  $\mathbf{Q}$ , the covariance matrix can be written as  $\boldsymbol{\Sigma} = \mathbf{Q} \mathbf{D} \mathbf{Q}^*$ . Therefore,  $\mathbf{Q}$  is the matrix of the eigenvectors of  $\boldsymbol{\Sigma}$  and  $\mathbf{D}$  is the vectors of the eigenvalues. One straightforward property is that  $\mathbf{Q} \mathbf{Q}^* = \mathbf{Q}^* \mathbf{Q} = \mathbf{I}$ .

As the eigenvalues are now clear, the matrix inversion is simplified to  $\boldsymbol{\Sigma}^{-1} = \mathbf{Q} \mathbf{D}^{-1} \mathbf{Q}^*$  and the determinant is  $|\boldsymbol{\Sigma}| = \prod_j \{g(\boldsymbol{\omega}_j) / (2\pi)^d\}$ . The log-likelihood of multivariate Gaus-

sian distribution can be expressed as (with the constant omitted):

$$-\frac{1}{2} \sum_{\mathbf{j} \in [1 \dots N_1] \times \dots \times [1 \dots N_d]} [\log(g(\boldsymbol{\omega}_{\mathbf{j}})) + \frac{(\mathbf{Q}\mathbf{Z})_{\mathbf{j}}(\mathbf{Q}^*\mathbf{Z})_{\mathbf{j}}}{g(\boldsymbol{\omega}_{\mathbf{j}})}] \quad (5)$$

The most important but understated property of this decomposition is that, the matrix  $\mathbf{Q}$  remains fixed for any weakly stationary process on a regular lattice. More specifically, regardless of the choice of covariance function, if weak stationarity is assumed, the covariance matrix on the lattice always has the same set of eigenvectors. Secondly, as  $\mathbf{Q}$  covers the discrete frequencies in  $[0, 2\pi)$  in each dimension, for any real or complex matrix  $\mathbf{A}$ ,  $\mathbf{Q}\mathbf{A}$  is equivalent to the normalized  $d$ -dimensional backward discrete Fourier transform (DFT) on  $\mathbf{A}$  and  $\mathbf{Q}^*\mathbf{A}$  is the normalized forward DFT; therefore, either direction can be evaluated with complexity of  $O(N \log_2 N)$  using the fast Fourier transform algorithm [Cooley and Tukey, 1965]. Since  $\mathbf{Z}$  is real,  $\mathbf{Q}\mathbf{Z}$  and  $\mathbf{Q}^*\mathbf{Z}$  are conjugate and only need one time invocation of DFT. As a result, there is no need for matrix inversion (an  $O(N^3)$  operation) nor matrix multiplication (an  $O(N^2)$  operation). The computation only involves linear operation on  $g(\boldsymbol{\omega}_{\mathbf{j}})$  and DFT.

Lastly, although commonly overlooked, one imperfection emerges in the above derivation in (3). For any subvector of  $\mathbf{x}$ , since  $x_k$  has increment of 1 and the location number  $N_k < \infty$ , a symmetry appears such that  $\cos(x_k \omega_k) = \cos((N_k - x_k) \omega_k)$  and  $i \cdot \sin(x_k \omega_k) = -i \cdot \sin((N_k - x_k) \omega_k)$ . It becomes necessary to have  $g(\omega_k) = g(2\pi - \omega_k)$  so that the imaginary terms can be canceled and  $C_a$  remains real. This duplication suggests that only  $N/2$  of the covariance (corresponding to the ones when the distance  $|x_k| \leq N_k/2$ ) are unique. This undesirable symmetry causes an artifact known as the edge effect. Fortunately, it can be easily ruled out with the augmentation of a few nuisance variables, as shown in the next section.

### 3 Functional Gaussian Process

Despite substantial computational advantages, Whittle's likelihood has seen very limited applications, presumably due to the following two restrictions: 1) The data number  $N$  needs to be sufficiently large such that the Riemann sums have high accuracy 2) the lattice needs to be complete such that  $\mathbf{Q}$  remains fixed. Initially, from a Bayesian perspective,

overcoming these restrictions seems easy, if we consider the data to be a partially observed lattice process. However, the sampling of the missing values would again require inversion of the matrix on the irregular lattice for the observed locations.

It becomes beneficial at this point to introduce the functional Gaussian process – a latent smooth surface underneath the noisy realization of the observed and missing values. Conditional on this process, the missing values can be updated easily; since the observed and missing values form a complete lattice, the process can be estimated as a smoother.

### 3.1 Modeling Structure

We define the functional Gaussian process  $\boldsymbol{\mu}$  as any Gaussian process such that its finite dimensional distribution on a lattice follows:

$$\boldsymbol{\mu} \sim \mathbf{N}_{(d)}(\mathbf{0}, \mathbf{QD}(\phi, \boldsymbol{\rho})\mathbf{Q}^*) \quad (6)$$

where  $N_{(d)}$  denotes a (possibly degenerate) multivariate Gaussian distribution,  $\mathbf{Q}$  is the constant matrix defined in (4),  $\mathbf{D}(\phi, \boldsymbol{\rho})$  is formed by the spectral density function with  $\phi$  as its scale parameter and  $\boldsymbol{\rho}$  as other parameters such as range.

Let  $\mathbf{Z}$  be the vector of interest, partitioned as observed data  $\mathbf{Z}_o$  and missing data  $\mathbf{Z}_m$ , and consisting of noisy realizations around  $\boldsymbol{\mu}$ :

$$\mathbf{Z} \sim \mathbf{N}(\boldsymbol{\mu}, \sigma^2\mathbf{I}) \quad (7)$$

We use  $\mathbf{Q}_j$  and  $d_j$  to denote the  $j$ th eigenvector and eigenvalue, respectively, in  $\mathbf{Q}$ . Then  $(\mathbf{Q}^*\mathbf{Z})_j$  is the  $j$ th element of the forward discrete Fourier transform on vector  $\mathbf{Z}$ , normalized by  $1/\sqrt{\prod_{k=1}^d N_k}$ . This implies the log-likelihood for  $\mathbf{Z}$  is:

$$-\frac{1}{2} \left\{ \sum_{j=1}^N \frac{(\mathbf{Q}^*\mathbf{Z})_j (\mathbf{Q}\mathbf{Z})_j}{(d_j + \sigma^2)} + \sum_{j=1}^N \log(d_j + \sigma^2) + N \log(2\pi) \right\} \quad (8)$$

It is worth noting that  $\boldsymbol{\mu}$  might be degenerate but the marginal likelihood of  $\mathbf{Z}$  is always defined. This is due to the notion that for  $\mathbf{Z}$ , its marginal covariance is  $\mathbf{QDQ}^* + \sigma^2\mathbf{I} = \mathbf{Q}(\mathbf{D} + \sigma^2\mathbf{I})\mathbf{Q}^*$ . In other words,  $\sigma^2$  is the lower bound of the eigenvalues for the covariance of  $\mathbf{Z}$ , even when some  $d_k$  can approach 0. It is possible to generalize  $\sigma^2$  to have different

values at different locations. For the sake of modeling simplicity, we restrict our focus to a common  $\sigma^2$ .

It appears striking that  $\boldsymbol{\mu}$  might be from a degenerate distribution. However, this is natural for a highly autocorrelated process without independent variation, where only  $m$  values can move freely ( $m$  is the rank of the matrix) and the remaining  $N - m$  values are simply deterministic. In such a case, it is more reasonable to consider this distribution as a degenerate multivariate Gaussian distribution. The lack of defined density in degenerate normal distributions can be solved by restricting the Lebesgue measure within the  $m$ -dimensional subspace; since the remaining  $N - m$  elements are deterministic, we define their conditional densities as a point mass given the previous  $p$  elements. This regularization enables us to have the clear definition for any conditional density given  $\boldsymbol{\mu}$ .

Acknowledging the possible singularity in the covariance of the underlying process  $\boldsymbol{\mu}$  helps clarify some problems one would encounter often in Gaussian process regression. Traditionally, one would have to put constraints on the parameters so that the covariance remains positive definite. However, in our parameterization, we can remove such constraints and allow the matrix to be positive semidefinite. Regardless, the likelihood (8) is not affected as the eigenvalues are  $\{d_j + \sigma^2\}$ , which are always positive.

To formulate  $\mathbf{D}$ , many widely used covariance functions have simple closed forms of spectral density, such as squared exponential or Matérn covariance. If no closed form exists, then the fast Fourier transform of the covariance function can be used as a numerical estimate. For the prior specification for hyper-parameters  $\phi$  and  $\boldsymbol{\rho}$ , the common proper diffuse prior can be used; more desirably, an objective improper prior can be used. As originally proposed by Berger et al. [2001], reference prior  $\{tr[\mathbf{W}_\rho^2] - \frac{1}{n-p}(tr[\mathbf{W}_\rho])^2\}^{1/2}/\phi$  with  $\mathbf{W}_\rho = ((\partial/\partial\rho)\boldsymbol{\Sigma})\boldsymbol{\Sigma}^{-1}(\mathbf{I} - \mathbf{X}(\mathbf{X}'\boldsymbol{\Sigma}^{-1}\mathbf{X})^{-1}\mathbf{X}'\boldsymbol{\Sigma}^{-1})$  can now be rephrased in the spectral domain such as  $\mathbf{W}_\rho = \mathbf{Q}\mathbf{D}_\rho\mathbf{D}^{-1}\mathbf{Q}^*(\mathbf{I} - \mathbf{X}(\mathbf{X}'\mathbf{Q}\mathbf{D}^{-1}\mathbf{Q}^*\mathbf{X})^{-1}\mathbf{X}'\mathbf{Q}\mathbf{D}^{-1}\mathbf{Q}^*)$ , which can be evaluated quite efficiently. Despite the unorthodox construction of the covariance matrix, the parameters used in the functional Gaussian process are the same as one would obtain with the traditional approach, including the sill, nugget, range, etc. This allows for convenient interpretation.

## 3.2 Posterior Sampling

The posterior sampling consists of three simple updating steps on the latent process  $\boldsymbol{\mu}$ , missing values  $\mathbf{Z}_m$  and covariance parameters  $\{\boldsymbol{\rho}, \sigma\}$ . We utilize Gibbs sampling to obtain the posterior estimates.

### 3.2.1 Latent Process and Missing Value Sampling

We sample the latent process  $(\boldsymbol{\mu}|\mathbf{Z}_m, \mathbf{Z}_o)$  and the missing values  $(\mathbf{Z}_m|\boldsymbol{\mu})$  from the following distributions:

$$\begin{aligned} (\boldsymbol{\mu}|\mathbf{Z}_m, \mathbf{Z}_o) &\sim \mathbf{N}_{(d)}(\mathbf{QD}(\mathbf{D} + \mathbf{I}\sigma^2)^{-1}\mathbf{Q}^*\mathbf{Z}, \mathbf{Q}(\mathbf{D} - \mathbf{D}(\mathbf{D} + \mathbf{I}\sigma^2)^{-1}\mathbf{D})\mathbf{Q}^*) \\ (\mathbf{Z}_m|\boldsymbol{\mu}) &\sim \mathbf{N}(\boldsymbol{\mu}_m, \mathbf{I}\sigma^2) \end{aligned} \quad (9)$$

where  $\boldsymbol{\mu}_m$  denotes the subvector of  $\boldsymbol{\mu}$  that corresponds to the missing location. For the first distribution,  $(\boldsymbol{\mu}|\mathbf{Z}_m, \mathbf{Z}_o)$  can be sampled by first generating two independent copies of vector of  $\mathbf{Y}_1, \mathbf{Y}_2 \sim \mathbf{N}(\mathbf{0}, \mathbf{D} - \mathbf{D}(\mathbf{D} + \mathbf{I}\sigma^2)^{-1}\mathbf{D})$ , then applying the transformation  $\mathbf{Y} = \mathbf{Re}(\mathbf{Q})\mathbf{Y}_1 + \mathbf{Im}(\mathbf{Q})\mathbf{Y}_2$ , where  $\mathbf{Re}$  and  $\mathbf{Im}$  denote the real and imaginary coefficient matrices, respectively. This is due to an equivalent representation of the covariance  $\mathbf{QKQ}^* = \mathbf{Re}(\mathbf{Q})\mathbf{KRe}(\mathbf{Q}^T) + \mathbf{Im}(\mathbf{Q})\mathbf{KIm}(\mathbf{Q}^T)$ , which is real. In either of the distributions, there is no direct involvement of matrix inversion nor matrix product so the sampling of  $\boldsymbol{\mu}$  and  $\mathbf{Z}_m$  can be done efficiently. Given the notion that the DFT is the most expensive operation, it is rather wasteful to run it for 4 times ( in  $\mathbf{Re}(\mathbf{Q})\mathbf{Y}_1, \mathbf{Im}(\mathbf{Q})\mathbf{Y}_2$  and  $\mathbf{QD}(\mathbf{D} + \mathbf{I}\sigma^2)^{-1}\mathbf{Q}^*\mathbf{Z}$ ). It can be shown that an equivalent operation is  $\boldsymbol{\mu} = \mathbf{Re}(\mathbf{Q}(\mathbf{Y}_1 - i\mathbf{Y}_2 + \mathbf{D}(\mathbf{D} + \mathbf{I}\sigma^2)^{-1}\mathbf{Q}^*\mathbf{Z}))$ , which only involves 2 times of DFT operations.

It might be tempting to sample the missing value  $\mathbf{Z}_m$  by directly updating from the conditional normal distribution  $\mathbf{N}(\mathbf{Z}_m|\mathbf{Z}_o)$ , with its variance:

$$\mathbf{Var}(\mathbf{Z}_m|\mathbf{Z}_o) = \mathbf{Q}_m\mathbf{DQ}_m^* + \mathbf{I}\sigma^2 - \mathbf{Q}_m\mathbf{DQ}_o^*(\mathbf{Q}_o\mathbf{DQ}_o^* + \mathbf{I}\sigma^2)^{-1}\mathbf{Q}_o\mathbf{DQ}_m^* \quad (10)$$

where we use  $\mathbf{Q}_o$  to denote the submatrix formed by the rows of  $\mathbf{Q}$  that corresponds to the row index of  $\mathbf{Z}_o$ ; we define  $\mathbf{Q}_m$  in the similar way for  $\mathbf{Z}_m$ . However, frequent evaluations of (10) are not feasible since  $\mathbf{Q}_o^*\mathbf{Q}_o \neq \mathbf{I}$ , the matrix inversion in (10) would need to be computed in the traditional way. This would create another bottleneck step. Such a

problem can be avoided with the latent process  $\boldsymbol{\mu}$ , since  $(\mathbf{Z}_m|\boldsymbol{\mu})$  are simply independent normal distributions.

### 3.2.2 Covariance Parameter Sampling

After obtaining the sample of the missing values in  $\mathbf{Z}_m$ , we resort to the likelihood stated in (8). Then the covariance parameters can be updated easily with the inverse-Gamma distribution for the scale parameters and Metropolis-Hastings criterion for the other ones. The complexity for these steps is only  $O(N)$ .

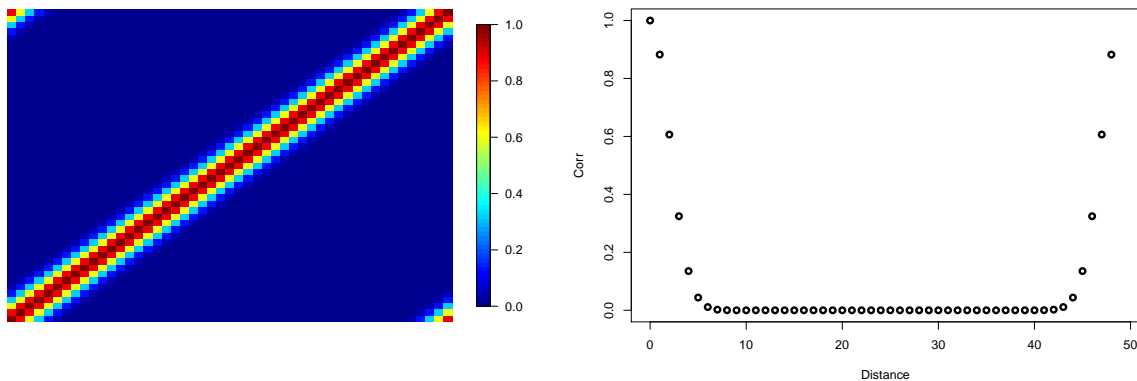
### 3.3 Edge Effect, Small $N$ and Remedy

Now we direct the focus to address the artifact called edge effect. When  $N \rightarrow \infty$ , the approximation in (3) approaches the true covariance function (2). However, in reality as we always observe  $N < \infty$ , a phenomenon we call edge effect will appear on the off-diagonal corners of matrix  $\mathbf{QDQ}^*$ : the observations on the two edges will show high correlation instead of 0 (Figure 1(a)). This is not a numeric artifact but rather a result of duplicate frequencies in the  $\mathbf{Q}$  matrix and use of the DFT. After the DFT, the period for the elements in each row or column in the matrix becomes  $N$  (Figure 1(b)). Since  $x$  is an integer, the element of the matrix representing the covariance with distance  $s$  is  $C(x) = \sum_{k=0}^{N-1} g(\frac{2\pi k}{N}) \cos(\frac{2\pi k}{N} s) = \sum_{k=0}^{N-1} g(\frac{2\pi k}{N}) \cos(\frac{2\pi k}{N} (N - x)) = C(N - x)$ . As shown in Figure 1(b), in the first row of the matrix, only the first  $N/2$  of the results are unique and the remaining  $N/2$  simply proceed as the reverse list. Fortunately, as most of the correlations after  $N/2$  are close to 0, only the last few exhibit an increasing behavior, which is the cause of edge effect.

Empirical solutions have been proposed, such as the work by Choudhuri et al. [2004]. These adjustments are commonly known as tapering, where smaller weights are placed on the edge values to diminish their impact on the likelihood estimation. This treatment is effective, but involves loss of information from the actual data on the edge.

In our model, since we propose an efficient mechanism for sampling missing values, we can simply augment the data of size  $N$  with additional  $N_{aug}$  missing values at the end. In this manner, we can sample these  $N_{aug}$  points as nuisance variables, which may have

high correlation with the other end of actual data; simultaneously, the correlation within the  $N \times N$  submatrix for the actual data will not have the edge effect. It is obvious that setting  $N_{aug} = N$  will double the number of unique variables and thus completely prevent the edge effect from appearing in the  $N \times N$  submatrix. In practice, since most of the repeated values are close to zero, one can set  $N_{aug}$  adaptively so that the last few numbers remain negligible. For this reason, we used this augmentation to circumvent the edge effect in all of the following studies.



(a) Edge effect arising from the duplicated frequencies in  $\mathbf{Q}$

(b) The first row of the matrix, in which the last few elements increase back to the second value and cause edge effect.

Figure 1: Illustration of edge effect using a  $50 \times 50$  matrix with squared exponential covariance and range  $\rho = 3$ . If the data of interest has size  $N = 50$  and no augmentation is used, then the edge effect on the corners would impact the likelihood. However, if the data of interest has size  $N \leq 40$  and  $N_{aug} = 50 - N$ , then the edge effect would have no impact on the likelihood of the  $N$  data.

Another concerning issue might be the case with small  $N$ . Indeed, the Riemann approximation relies on large  $N$  for good accuracy, and a previous study [Fuentes and Smith, 2001] suggested the minimum requirement of  $N > 100$  for a good approximation. In a Bayesian framework, however, we can solve this issue similarly by setting up a larger lattice, in which only  $N$  points are actually observed and the rest are missing. In numerical studies we found that, if the noise variance  $\sigma^2$  is reasonably small, the range estimation

can still be quite accurate even with an observed  $N$  as low as 20 (using  $N_{aug} = 180$  points as missing). We found that the fitting with  $N < 20$  is too sensitive to the choice of the hyperparameter prior and hence not recommended.

## 4 Comparison with Other Gaussian Process Approaches

Now we compare the functional Gaussian process, a Bayesian spectral approach, with its counterparts using maximum likelihood estimation (MLE) or using a standard Bayesian approach that involves direct matrix inversion.

The most commonly used approaches are the exact maximum likelihood estimation (MLE(E)) and Bayesian Gaussian process (BGP). These methods are well studied and have been implemented in software, such as the “fields” [Furrer et al., 2009] and “spBayes” [Finley et al., 2007] packages in R. If computational cost could be disregarded, they seem optimal for parameter estimation. However, one significant caveat lies in the possible matrix singularity and the subsequent failure in the matrix inversion, caused by relatively high correlation in the Gaussian process. In such cases, these implementations either directly fail or converge to a much smaller range estimate driven by a false upper bound restriction. In our test sample, neither of the aforementioned packages could estimate a squared exponential Gaussian process with range  $\rho = 3$  and nugget/sill ratio  $\sigma^2/\phi \leq 6\%$ . On the other hand, this does not mean such methods are intractable for highly correlated data. Similar to the rationale we presented in Section 3, it is reasonable to consider that the latent process follows a possibly degenerate multivariate distribution, as long as the realized process has a positive definite covariance matrix. Therefore, as the common remedy to the matrix singularity problem, one needs to format the likelihood using the sum of Gaussian process covariance and the diagonal nugget matrix (noise variance). A more persuasive reason can be obtained from the spectral point of view – the nugget becomes the lower bound for the smallest matrix eigenvalue, thereby guaranteeing that the matrix will be well-conditioned and invertible.

Following this recipe, we implement the MLE(E) and BGP approaches. For MLE(E) optimization, we used the Newton-Raphson algorithm, which treats the likelihood as the objective function and the analytical first derivation as the search direction. For the second

derivatives, we use the finite difference approach to compute the Hessian matrix. We use the ridge-stabilized technique [Perrett, 2010] to avoid numerical singularity and improve convergence. For the BGP approach, we use flat priors and sample the posterior distribution using the Metropolis-Hastings algorithm.

A third method for comparison with our approach is the spectral MLE [Fuentes, 2007]. The authors provide an approximate equation to the likelihood of the data with missing entries. We denote this method as MLE(S). The adjustment is achieved through zero fill-ins at missing location, which leads a modified version of the Whittle’s likelihood [Whittle, 1953]. Their study finds good approximation with missing proportions that are less than 20%. We generated data using squared exponential covariance with the same set of parameters and then test the four model on a 1-dimension (1D) and 2-dimension (2D) grids.

In 1D setting, we generated 1,000 data entries, which is relatively large to have good precision for the spectral approximation. We list the point estimates for the parameter point and their standard deviations in Table 1. Among the four, MLE(S), BGP and FGP all provide good results, where the latter two show slightly better accuracy. The surprise we encountered is that the MLE(E) estimates are highly sensitive to the starting values. Even from a starting point close to the true values (for all the MLE(E) results, we used starting points  $\{2.8, 120, 8\}$ ), the parameter would have a large Hessian matrix and the optimization appeared to be stuck at local convergence. We switched to the conjugate gradient approach and it still showed no improvement. This hampers further optimization for the MLE(E). Due to this reason, we conclude the MLE(E) is the least favorable choice among the four approaches and exclude it from the following comparison.

In the 2D setting, we set up a  $50 \times 50$  grid. In each direction, 50 is a small number so that it may affect the precision of the spectral approaches. As a result, MLE(S) does exhibit a distorted estimate in the range  $\rho$ . On the other hand, while FGP is another spectral approach, it is easy to set up a larger lattice with missing points (in this case, we set up additional  $N_{missing} = 50$ ), which effectively increased the grid to  $100 \times 100$  and preserved the accuracy. As it shows in the table, the FGP and BGP results are almost the same. Surprisingly in most occasions, FGP provides even more accurate results than BGP, possibly due to the larger numerical error of matrix inversion in BGP (more will be

Setting	Method	$\rho$	$\phi$	$\sigma^2$
	True Value	3	150	10
1D Squared Exp (1,000 data points with 0 missing)	MLE(E)	2.92 (0.05)	130.3 (6.7)	9.8 (0.9)
	MLE(S)	2.95 (0.08)	171.2 (10.0)	9.9 (0.5)
	BGP	2.93 (0.09)	131.4 (14.3)	10.8 (0.5)
	FGP	3.01 (0.09)	161.6 (16.2)	10.4 (0.5)
2D Squared Exp (50 × 50 data points with 0 missing)	MLE(E)	2.91 (0.03)	130.0 (7.5)	10.8(0.2)
	MLE(S)	2.69 (0.07)	133.1 (14.1)	12.8 (0.3)
	BGP	3.03(0.06)	154.7 (14.3)	10.4 (0.3)
	FGP	3.00(0.06)	158.7 (14.7)	9.7 (0.3)
1D Squared Exp (1,000 data points with 15% missing)	MLE(E)	2.79 (0.06)	130.3 (6.6)	10.4(0.1)
	MLE(S)	2.92 (0.08)	122.3 (10.0)	21.4 (0.8)
	BGP	2.92 (0.10)	137.4 (14.1)	9.8 (0.5)
	FGP	3.05 (0.10)	139.3 (13.8)	10.2 (0.6)
2D Squared Exp (50 × 50 data points with 15% missing)	MLE(E)	2.91 (0.07)	130.0 (7.6)	10.8 (0.1)
	MLE(S)	2.75 (0.07)	93.2 (32.9)	26.2 (0.8)
	BGP	2.91 (0.07)	143.3 (16.5)	10.0 (0.3)
	FGP	3.02(0.07)	142.3 (16.4)	10.5 (0.3)
1D Squared Exp (1,000 data points with 50% missing)	MLE(E)	2.82 (0.08)	130.1 (8.3)	10.9 (0.1)
	MLE(S)	3.39 (0.24)	53.6 (1.0)	45.1 (2.6)
	BGP	3.05 (0.12)	124.3 (18.2)	10.9 (0.8)
	FGP	3.01 (0.13)	168.9 (17.4)	10.3 (0.8)
2D Squared Exp (50 × 50 data points with 50% missing)	MLE(E)	2.89 (0.08)	130.1 (6.2)	10.8 (0.1)
	MLE(S)	2.87 (0.12)	51.1 (1.0)	40.4 (0.7)
	BGP	2.95 (0.08)	133.1 (14.7)	9.7 (0.5)
	FGP	2.97 (0.07)	135.5 (15.3)	9.4 (0.4)

Table 1: The parameter estimates from the 4 methods. The numerical accuracy of the methods can be ranked as FGP>BGP>MLE(E)>MLE(S).

discussed in the last section).

We then gradually delete observations so that the observation pattern no longer appears to be regularly spaced. For MLE(E) and BGP, this reduces the size of the covariance matrix to the observed locations only; for FGP, it increases the number of missing values;

for MLE(S), this changes its likelihood formulation with zero fill-ins. As shown in the results, 15% of missingness has no effects on BGP and FGP, but has an obvious impact on MLE(S), especially on  $\phi$  and  $\sigma^2$ , likely due to the downscaling of possible missing values to 0. The range estimate for  $\rho_x$  using MLE(S) is either biased upward or downward. It is worth noting that such bias for  $\rho_x$  with MLE(S) is not severe even at a missing data rate of 50%, which supports using MLE(S) as a quick approximate solution. Among all, FGP and BGP have the highest accuracy in estimating the parameters.

In computational time, BGP is the slowest and took 25 minutes to fit the 1D data (1,000 entries) and 6 hours to fit the 2D data (2,500 entries), each with 2,000 MCMC steps; MLE(E) is second due to its slow converge rate. FGP is much more efficient. For 1D data, it took about 4 seconds for 2,000 steps; for 2D data, it took about 9 seconds. In terms of the time to achieve convergence, MLE(S) is the fastest and took about 3 seconds. The time difference between FGP and BGP, as well as MLE(S) and MLE(E), is huge but not unpredictable, since the computational load is in  $O(N \log_2(N))$  and  $O(N^3)$ , respectively.

To summarize this comparison study, the Bayesian approach tended to yield more accurate estimates for the Gaussian process parameters. The functional Gaussian process (FGP) has an equivalent or higher level of accuracy compared with the traditional Bayesian approach (BGP) and is substantially more computationally efficient. The spectral approximation of maximum likelihood (MLE(S)) is the fastest estimation approach, but its accuracy was compromised when sample size is small or missingness occurred. The traditional exact maximum likelihood method (MLE(E)) suffers from local convergence, therefore its results were questionable unless reasonable starting values were chosen.

## 5 Generalized Functional Gaussian Process

In real-world data, non-stationarity and non-Gaussianness are common. We now extend the functional Gaussian process to accommodate these assumptions. We demonstrate how the latent process can facilitate the extended model.

In the peer studies, various approaches have been proposed to accommodate non-stationarity, such as the weighted average of locally stationary processes [Fuentes and Smith, 2001] or process convolution [Higdon, 1998]. A similar approach to these meth-

ods is to have the parameters vary by locations, which has been studied by Paciorek and Schervish [2006] and Anderes and Stein [2011]. Our generalized approach allows each location to have its own parameters; however, in some subgroup of locations (such as in a small local region), these parameters show similarity and therefore can be considered as “clustered”. Under this assumption, a Dirichlet process can be adopted to create an infinite mixture of stationary processes. Specifically, one can consider an autocorrelated process at location  $s$  with measure:

$$Pr(Z(s)) = \sum_{l=1}^{\infty} \omega_l(s) \delta_l(s, Z_s) \quad (11)$$

where  $\{\delta_l\}$  for  $l = 1, 2, \dots$  is a collection of independent stationary Gaussian process densities defined on  $s$ ;  $\omega_l$  is a set of independent weights, which can be described through stick-breaking construction [Ishwaran and James, 2001] such that  $\omega_l = \nu_l \prod_{k<l} (1 - \nu_k)$  and  $\nu_k \sim Beta(1, \alpha)$  for  $k = 1, 2, \dots$  (to avoid any confusion with the variable in the frequency space, unless otherwise stated,  $\omega$  only denotes the weight in the following context). The generated random field is very flexible, as it not only accommodates non-stationarity, but is also capable of addressing non-Gaussian scenario as it yields a mixture distribution.

It is worth noting that for different  $s$ , the distribution of  $\delta_l(s)$  is correlated as in a stationary Gaussian distribution, so the vector of  $\mathbf{Z}$  across different  $s$  is a dependent Dirichlet process [MacEachern, 2000]. A more realistic consideration is that the weights  $\{\omega\}$  should also be autocorrelated as locations vary, for which Duan et al. [2007] proposed an improved model known as the generalized spatial Dirichlet process. This is important in guaranteeing the smoothness of the posterior mean vector, for which the marginal expectation of  $\mathbf{Z}$  in (11) is  $\sum_l \omega_l \mu_{zl}$  and requires smoothness in both  $\mu_{zl}$  and  $\omega_l$ .

Motivated by these studies, we propose the following generalized model, which takes full advantage of the conveniences from the functional Gaussian process. For each  $l$ , We use  $\boldsymbol{\nu}_l$  to denote the vector of stick breaking probabilities and  $\mathbf{Z}_l$  to denote the realization from the stationary  $\delta_l$ . Unlike Duan et al. [2007] who addressed the weight correlation in  $\Phi^{-1}(\boldsymbol{\nu}_l)$  with a constant mean and a correlation matrix, we assume  $\Phi^{-1}(\boldsymbol{\nu}_l)$  has a flexible mean but independent noise variance equal to 1. This leads to our formation of the generalized

functional Gaussian process:

$$\begin{aligned}
Z(s) &= Z_l(s) \text{ w.p. } \nu_l(s) \prod_{k < l} (1 - \nu_k(s)) \\
\mathbf{Z}_l &\sim \mathbf{N}(\boldsymbol{\mu}_{z_l}, \mathbf{I}\sigma^2) \\
\boldsymbol{\nu}_l &= \Phi(\boldsymbol{\mu}_{\nu_l})
\end{aligned} \tag{12}$$

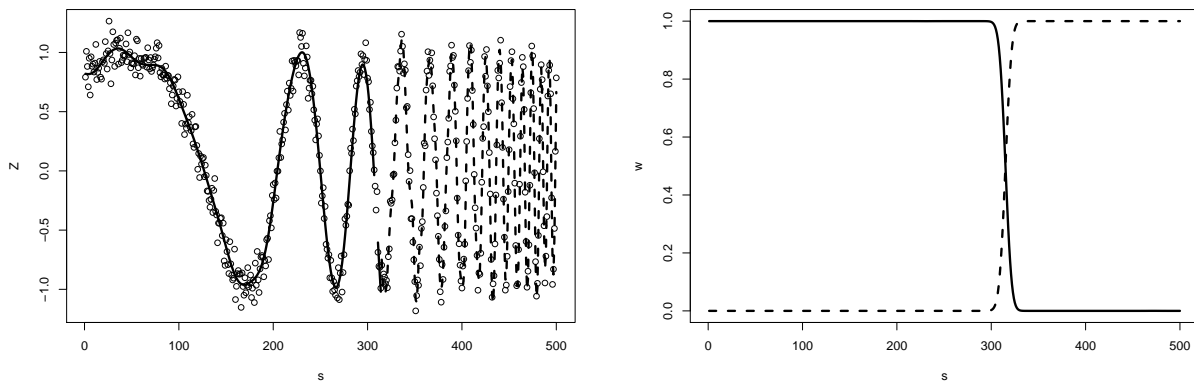
where  $\boldsymbol{\mu}_{\nu_l}$  and  $\boldsymbol{\mu}_{z_l}$  are two independent functional Gaussian processes as defined in (6),  $\Phi$  is the transformation of a probit function applied on each element in  $\boldsymbol{\mu}_{\nu_l}$ . For the  $l$ th component, we use  $\boldsymbol{\theta}_{z_l}$  and  $\boldsymbol{\theta}_{\nu_l}$  to denote the parameters (such as range and sill) in the two functional Gaussian processes.

The model structure in (12) makes it very easy and efficient to sample the posterior distribution. For each component  $l$ , there are two functional Gaussian processes, since they can be conditioned on two separate sets of parameters, they are sampled with conditional independence. Also, the updating inside components with different  $l$ 's are also independent and therefore can be done in parallel. As a result, the total computational complexity is still  $N \log_2(N)$ .

Besides the computational benefit, the two functional Gaussian processes  $\boldsymbol{\mu}_{(\cdot)}$  are essential in the posterior sampling. Firstly, the latent auxiliary variables in a probit link function would involve a correlated truncated Gaussian distribution, as first discovered by Albert and Chib [1993] in the univariate case and later extended to the multivariate case by Duan et al. [2007]. The sampling of such a distribution is difficult; however, when conditioned on  $\boldsymbol{\mu}_{\nu_l}$ , the truncated multivariate distribution is converted to that of an independent truncated Gaussian vector. Secondly, the calculation of the probability of assigning a data point to a certain component might be difficult. When considering  $\boldsymbol{\mu}_{z_l}$  as the parameter for the  $l$ th component, it is easy to compute  $Pr(Z_s | \boldsymbol{\mu}_{z_l})$  as part of the probability for the multinomial choice. We list the sampling algorithm in the appendix.

## 5.1 Illustrative Examples

In order to illustrate the identifiability of the generalized model (GFGP), we carried out simulations using two types of data from: (1) a non-stationary Gaussian process; (2) a multimodal stochastic process.



(a) The simulated data evolving in increasing frequencies, where the proposed model converged to a posterior mean consisting of 2 stationary regions.

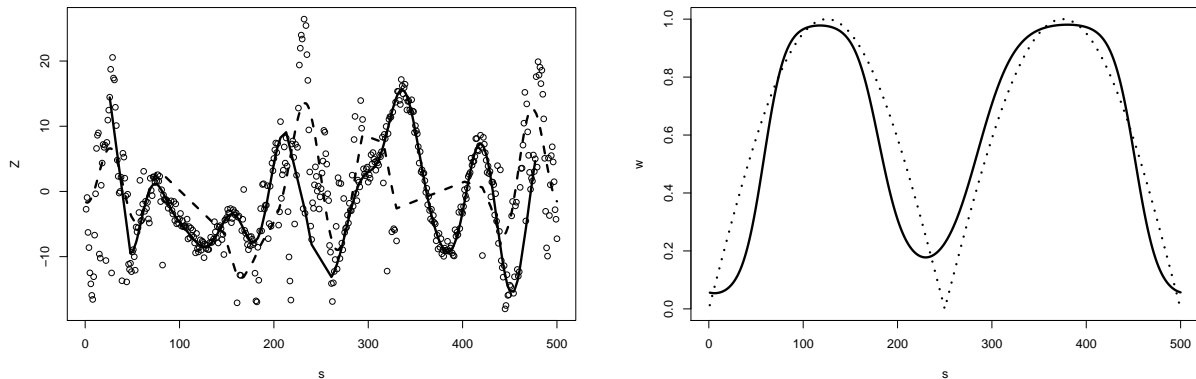
(b) The estimated weights for the 2 regions; line types are consistent with those on the left.

Figure 2: Simulation of a nonstationary Gaussian process:  $Z(s) = \sin(\exp(s \cdot \pi / 500 / 0.7)) + \epsilon_s$ ,  $\epsilon_s \stackrel{iid}{\sim} N(0, 0.01)$  for  $s = 1, 2, \dots, 500$

For the first type, we generated data with a trigonometric function, for which its frequency increases exponentially as  $s$  increases. Although the frequency is different for each data point, the differences within a small region would be negligible so the corresponding data appear to be stationary. This is the reason our proposed model can cluster a nonstationary process using a finite number of stationary components. As shown in Figure 2(a), the discovered two regions clearly have distinct frequencies, yet within each region the difference is more subtle. The correlated weights are estimated with a curve that shows a switch in the middle.

For the second type, we generated data directly from a bimodal mixture of Gaussian processes. As shown in Figure 3 (a), the Gaussian pattern becomes indistinguishable once the data are mixed. Our proposed model correctly identified the two stationary means. We also compare the estimated weights and the real weights (Figure 3 (b)).

It is interesting that even though we carried out two different types of simulations, the model we used is the same one. This suggests that the GFGP is a very flexible model and may provide some guidance in the interpretation. If the estimated weights exhibit quick



(a) The simulated data exhibiting a non-Gaussian pattern that lacks an obvious mean curve, for which the proposed model converged to a random mixture of 2 stationary Gaussian processes.

(b) The estimated weights (solid line) for choosing the  $l = 1$  from the two components, compared with the true weights  $\omega_{l=1}$  (dots).

Figure 3: Simulation of a nonstationary and non-Gaussian process: a mixture of two stationary Gaussian processes with two different frequencies and mixture weights  $\omega_{l=1}(s) = |\sin(s \cdot 2\pi/500)|$

transition between 0 and 1 (as in case 1), it suggests the data is non-stationarily Gaussian; if the weight transition is smoother and slower (as in case 2), it suggests the data are non-Gaussian or from mixture distribution.

## 6 Application: Prediction in the Spatial-Temporal Data

We now apply the generalized functional Gaussian process on a complex system using a large spatial-temporal dataset. The data are obtained from the North American Regional Climate Change Assessment Program (NARCCAP). We use the surface air temperature in the North America region collected during 1971-2000 [Mearns et al., 2011]. The data are simulations from the Weather Research & Forecasting regional model (WRF) coupled with the Third Generation Coupled Global Climate Model (CGCM3). To exclude possible seasonal effects, we choose the annual average in each summer, which spans from June 21

to September 21, as the yearly measurement on a  $134 \times 109$  dense grid over 30 years. This results in 438,180 data points. We assume the observed temperature  $Z$  at location/time point  $s$  is

$$Z(x_s, y_s, t_s) = \beta^T X(x_s, y_s, t_s) + \mu(x_s, y_s, t_s) + \epsilon(x_s, y_s, t_s)$$

where  $x, y, t$  represent the induces of longitude, latitude and year, respectively; the term  $X$  is a fixed linear term which contains the intercept, first and second order terms of  $x, y, t$ ; the second term  $\mu(x_s, y_s, t_s)$  is assumed be a generalized functional Gaussian process, which is a mixture of stationary processes such that  $Pr\{\mu(x_s, y_s, t_s) = \mu_{zl}(x_s, y_s, t_s)\} = \Phi(\mu_{vl}(x_s, y_s, t_s)) \prod_{k < l} (1 - \Phi(\mu_{vk}(x_s, y_s, t_s)))$ ; the last term  $\epsilon(x_s, y_s, t_s)$  represents the noise, which is assumed  $\epsilon(x_s, y_s, t_s) \stackrel{iid}{\sim} N(0, \sigma^2)$  for all  $s$ .

One important use of the spatial-temporal models is their inference about the underlying process  $Y = \beta^T X + \mu$ . As described by Cressie et al. [2010], with data  $Z$  available at  $\{t_1, \dots, t_n\}$ , three types of prediction can be defined: the one about  $Y$  at  $t_k < t_n$  is called smoothing; the one about  $Y$  at  $t_k = t_n$  is called filtering; and the one about  $Y$  at  $t_k > t_n$  is called forecasting. We use them as the evaluation criteria for the spatial-temporal models.

The simplest choice of spatial-temporal model is to keep the spatial and temporal effects separate and additive, such that  $\mu(x_s, y_s, t_s) = \mu_1(x_s, y_s) + \mu_2(t_s)$ . In our case, we use the following covariance function:

$$Cov\{(x_s, y_s, t_s), (x_{s'}, y_{s'}, t_{s'})\} = \phi_1 \exp\left(-\frac{|x_s - x_{s'}|^2}{2\rho_x^2} - \frac{|y_s - y_{s'}|^2}{2\rho_y^2}\right) + \phi_2 \exp\left(-\frac{|t_s - t_{s'}|}{\rho_t}\right)$$

where the first exponential term is the anisotropic spatial covariance and the last one is the temporal term. We denote this model as  $M(A)$ . The advantage is that in multiple-step forecasting, when temporal correlation is weak, the spatial term remains unaffected. This sampling for this method is simple and the covariance matrix is kept on a manageable scale, with conditional sampling of the two additive terms. However, this model completely ignores the time-space interaction and may exhibit poor goodness-of-fit, which can affect the smoothing and filtering performances.

Another modification is to let the spatial effects diminish as the time distance increases. This can be achieved by multiplying the spatial and temporal covariance as the covariance.

In this study, we use:

$$Cov\{(x_s, y_s, t_s), (x_{s'}, y_{s'}, t_{s'})\} = \phi \exp\left(-\frac{|x_s - x_{s'}|^2}{2\rho_x^2} - \frac{|y_s - y_{s'}|^2}{2\rho_y^2}\right) \cdot \exp\left(-\frac{|t_s - t_{s'}|}{\rho_t}\right)$$

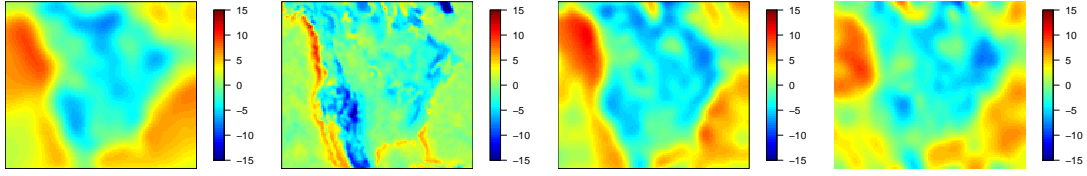
We refer this model as  $\mathbb{M}(S)$ . Although this model might not accommodate the need for long-term forecasting, the covariance is more realistic and may benefit in smoothing and filtering. Dimension reduction technique can be applied on this model. As shown by Banerjee et al. [2004], the matrix can be written as a Kronecker product of two smaller matrices that represent the spatial and temporal covariances. Therefore,  $\mathbb{M}(S)$  is a separable model. The drawback of this model is that it still assumes no interaction in the covariance and hence may be too limited to fit the data well.

A third class of spatial-temporal covariance was proposed by Cressie and Huang [1999] and later extended by Gneiting [2002]. They introduce additional time-space interaction terms into the covariance function. For example, we use the following construction:

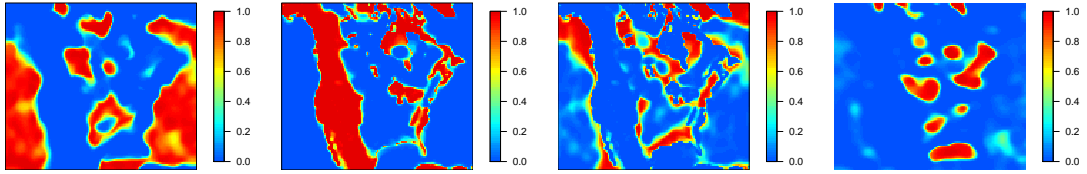
$$Cov\{(x_s, y_s, t_s), (x_{s'}, y_{s'}, t_{s'})\} = \phi \exp\left(-\frac{|x_s - x_{s'}|^2}{2\rho_x^2} - \frac{|y_s - y_{s'}|^2}{2\rho_y^2}\right) \cdot \exp\left(-\frac{|t_s - t_{s'}|}{\rho_t}\right) \\ \cdot \exp\left(-\frac{|x_s - x_{s'}|^2 |t_s - t_{s'}|}{c_1} - \frac{|y_s - y_{s'}|^2 |t_s - t_{s'}|}{c_2}\right),$$

where  $c_1 \geq 0$  and  $c_2 \geq 0$ . We refer this model as  $\mathbb{M}(NS)$ . This class of covariance is quite flexible in its interaction terms. When  $c_1$  or  $c_2$  are within moderate magnitude, the model describes a non-separable spatial-temporal process; when  $c_1 \rightarrow \infty$  and  $c_2 \rightarrow \infty$ , the model reduces to separable model. The added flexibility seems ideal for smoothing and filtering, but the non-separable nature of the covariance functions creates huge matrix. For our data, this would result in an matrix of size  $438,180 \times 438,180$ , which was impossible to handle by modern computers. However, this problem can be easily solved by the GFGP model that we propose.

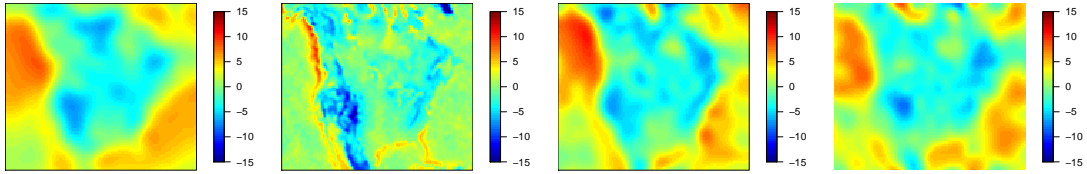
We computed the Fourier transform of the three covariance functions (see appendix) and tested the three models on the data. In order to evaluate the forecasting performance, we masked all the observations in 1996-2000 and sampled them as missing. The posterior means of the  $\beta^T X + \sum_l \omega_l \mu_{zl}$  at each location is used as the smoothing and filtering for 1990-1995 and the forecasting estimates for 1996-2000. For each, we ran MCMC sampling for 30,000 steps and use the last 20,000 steps as the posterior sample. The simplest model



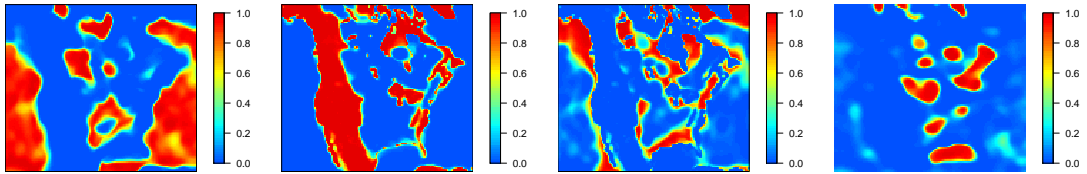
(a) Four stationary components at the year of 1990



(b) Corresponding weights to the four components at the year of 1990



(c) Four stationary components at the year of 1995



(d) Corresponding weights to the four components at the year of 1995

Figure 4: The four stationary components estimated by the time-space interactive model  $\text{M}(NS)$  using generalized functional Gaussian process (GFGP) model. The estimated mean process  $\boldsymbol{\mu}_k$  and weight process  $\boldsymbol{\omega}_k$  in each component are shown. Each mean processes  $\boldsymbol{\mu}_k$  has distinct smoothness and exhibits changes over the time; while each weight process  $\boldsymbol{\omega}_k$  shows geographical clustering and appears unchanged over time.

$\mathbb{M}(A)$  took about 20 minutes and the most sophisticated  $\mathbb{M}(NS)$  took about 9 hours. The computation time is indeed scaled in the order of  $O(N \log_2(N))$ .

In the results, both  $\mathbb{M}(A)$  and  $\mathbb{M}(S)$  converged to 3 dominating components and  $\mathbb{M}(NS)$  converged to 4 components. As the results are similar, we demonstrate the ones for  $\mathbb{M}(NS)$  here (see Figure 4, its parameter estimates are listed in the appendix). The component means  $\mu_{zl}$  have different range parameters, therefore have different degree of smoothness. The temporal parameters  $\rho_t$  for  $\mu_{zl}$  are relatively large and imply strong temporal correlation. As compared between (a) and (c) in Figure 4, an evolution of temperature pattern can be observed from 1990 to 1995, but this change is very subtle.

For the weight distribution  $\omega$ , the transform of  $\mu_{vl}$ , the spatial range parameters  $\rho_x$  and  $\rho_y$  are similar to the ones of  $\mu_{zl}$ . The autocorrelation of weight guarantees the smoothness of the allocated sub-domains, as shown in Figure 4(b) and (d). This not only ensures the weighted average  $\sum_l \omega_l \mu_{zl}$  is smooth, but also helps in a better interpretation of the model. The 1st component represents mostly the oceanic areas, the 2nd does the both coastal areas and the 3rd and 4th do the rest. Compared with the change in component means, the temporal change in component weights from (b) and (d) is hardly noticeable, thanks to the high values in range  $\rho_t$ . This suggests that the system mainly evolve through time by changing each stationary component, with their weights fixed.

Model	Metric	1991	1992	1993	1994	1995
$\mathbb{M}(A)$	RMSE	0.78	0.86	0.80	0.89	0.69
	MAD	0.43	0.46	0.45	0.48	0.38
$\mathbb{M}(S)$	RMSE	0.43	0.43	0.45	0.43	0.40
	MAD	0.18	0.17	0.18	0.17	0.16
$\mathbb{M}(NS)$	RMSE	0.42	0.43	0.44	0.43	0.39
	MAD	0.16	0.14	0.16	0.17	0.15

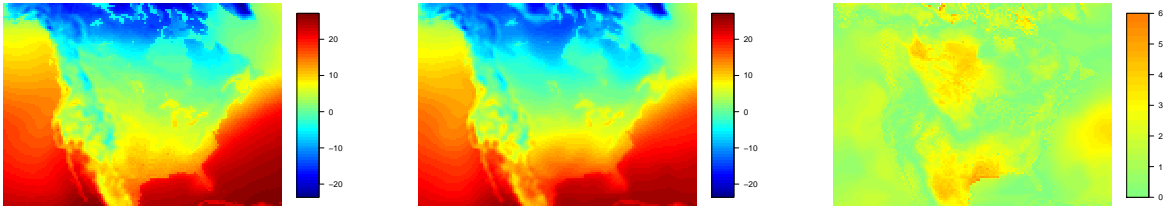
Table 2: The temperature smoothing errors for 1991-1994 and filtering errors for 1995. The time-space interactive model  $\mathbb{M}(NS)$  fits the data mostly well.

We list the prediction errors during 1991-1995 and 1996-2000 in Table 2 and 3. We use the root-mean-square error (RMSE) and median absolute deviation (MAD) as the metrics. The additive model  $\mathbb{M}(A)$  show its advantage in forecasting with the smallest forecasting

Model	Metric	1996	1997	1998	1999	2000
$\mathbb{M}(A)$	RMSE	2.02	1.30	1.43	1.81	1.16
	MAD	0.89	0.75	0.46	0.84	0.71
$\mathbb{M}(S)$	RMSE	1.54	1.12	1.33	1.50	1.65
	MAD	0.96	0.70	0.85	1.08	1.16
$\mathbb{M}(NS)$	RMSE	1.70	1.80	1.85	2.39	2.91
	MAD	1.22	1.36	1.53	1.97	2.57

Table 3: Forecasting errors for the temperature in 1996-2000. The simpler models  $\mathbb{M}(A)$  and  $\mathbb{M}(S)$  show better forecasting results.

errors in long range. The more complex models  $\mathbb{M}(S)$  and  $\mathbb{M}(NS)$  do not produce better forecasts, but they have better fit to the data and therefore is more suitable for smoothing and filtering purpose. With the space-time interaction, the non-separable model  $\mathbb{M}(NS)$  shows a slight improvement over the separable  $\mathbb{M}(S)$  in performance. For illustration, we plot the prediction map of temperature data of the year 1996 in Figure 5.



(a) The temperature data in 1996 in the original dataset. The unit is in Celsius. (b) The predicted values as the sum of the weighted average and the trend term,  $\mathbf{X}\beta + \sum_l \boldsymbol{\mu}_{\nu l} \Phi(\boldsymbol{\mu}_{z l})$ . (c) The absolute deviation between the real and predicted values, with the maximum difference at 6.44 Celsius.

Figure 5: Comparison of the original temperatures in the dataset and the predicted ones generated by the space-time interactive model  $\mathbb{M}(NS)$ .

Lastly, it is interesting to compare how covariance decays over time and location in model  $\mathbb{M}(S)$  and  $\mathbb{M}(NS)$ . As illustrated in Figure 6, in  $\mathbb{M}(S)$  the effects of  $x^2$  and  $|t|$  on the covariance are independent, which results in linear contour in covariance; whereas

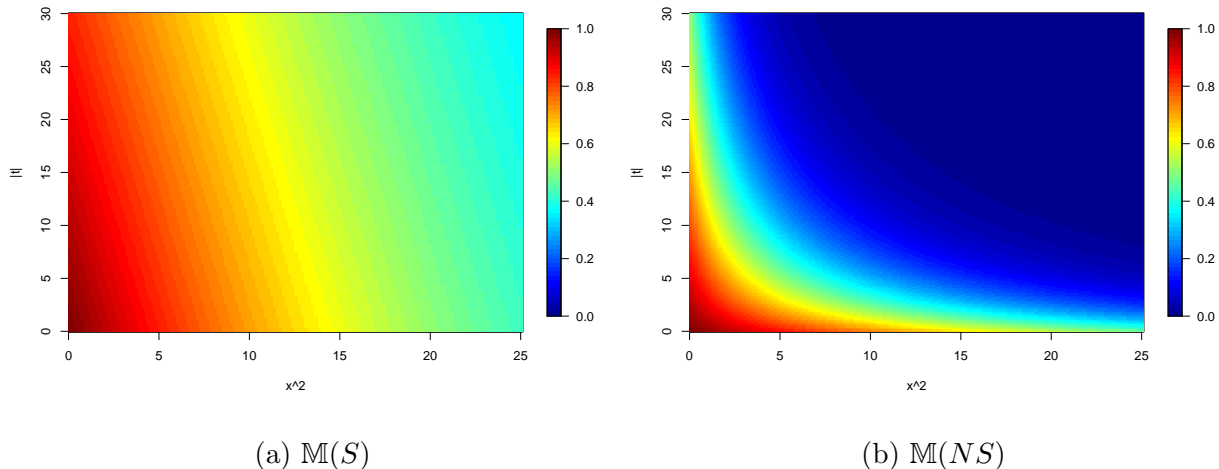


Figure 6: Plot of the covariance as the space distance  $x^2$  or the time distance  $|t|$  increases.

$\mathbb{M}(NS)$  has an interaction effect between space and time, which generates a curvature. It is interesting that in the latter, we only have  $c^* = 1/c = 0.01$ , but the interaction is very obvious. The coefficient  $c^* = 1/c$  was used in the original parameterization of  $\mathbb{M}(NS)$  by Cressie and Huang [1999]. And they interpreted that the interaction is negligible when  $c^*$ 's are close to zero. In their data application, surprisingly, the most fitted model was the one with  $c^* = 0$  and therefore they concluded no interaction was present. However, we found that a small  $c^*$  can sometimes be misleading. Indeed, it can be observed in the spectral density of  $g_{\mathbb{M}(NS)}$  that the interaction term between  $x^2$  and  $|t|$  would not disappear unless  $\rho_x^2|t|/c_1$  as a whole is close to 0 (see the appendix). In another words, if  $\rho_x$  is large (i.e. spatial association is strong), small  $c^*$  (or equivalently, large  $c$ ) does not exclude the existence of possible space-time interaction. Compared with  $c^* = 1/c$  alone, the ratio term in the spectral density (such as  $\rho_{(\cdot)}^2/c$ ) might be a better criterion. In the shown illustration, the calculated  $\rho_x^2/c$  is 0.37, which is the cause of the curvature. The space-time interaction model shows a quite interesting pattern of change in correlation. The estimation on this large dataset would not be possible without the conveniences provided by the GFGP framework.

## 7 Discussion

The idea of describing the Gaussian process through its spectral density is not new. The early studies can be dated back to half a century ago [Whittle, 1953, Ibragimov, 1963]. Despite the ease in obtaining estimates in the frequency domain, this method has seen very limited application in statistics, where we mainly focus on the observational domain. The main reason is that, unlike in the field of signal processing, the data we encounter in statistics are often noisy, irregularly located and have varying sample size. All of these characteristics prevent a good and accurate utilization of the discrete Fourier transform (DFT), which is essential in spectral studies.

We tackled these obstacles through a Bayesian latent variable framework. We assumed the observational data are only the partial and noisy realization from a large, regularly spaced and smooth process surface (which we call the functional Gaussian process). By sampling the missing values and the underlying process, we satisfy the data requirement for DFT and allow a valid integration of spectral density into the likelihood. The benefits are significant: the numerical accuracy is ensured through large  $N$ , the computational complexity is dramatically reduced and it allows feasible application of the Gaussian process approach on extremely large datasets and/or rather sophisticated models.

Similar to our work, some other spectral methods have also been proposed recently. Lázaro-Gredilla et al. [2010] model the Gaussian process as a linear combination of trigonometric functions, which are equivalent to the real and imaginary parts in the eigenvectors that we used; Stroud et al. [2014] use similar spectral decomposition in the likelihood and use the conjugate gradient to invert the partial covariance matrix. Compared with these approaches, our major contribution is the setup of the underlying smooth process  $\boldsymbol{\mu}$ , which enables simpler missing value sampling and provides a useful tool for various extensions, such as the link to discrete data regression and our mixture model generalization.

One possible concern may be the numerical precision of the FGP model, which was also the cause that motivated us to perform comparisons in the simulation studies. Not only did FGP correctly identify the true value parameters, but more surprisingly, its estimates seem even more accurate than the best existing approach (BGP) (Table 1). One likely explanation lies in the numerical analyses of the two methods. When the Gaussian process has

high autocorrelation, its covariance matrix is ill-conditioned with a large condition number  $\kappa = |\max \lambda / \min \lambda|$ , where  $\lambda$ 's are the eigenvalues of the matrix to be inverted. Specifically, larger  $\kappa$  leads to larger numerical error in matrix inversion [Cheney and Kincaid, 2012] and it usually increases with the size of the matrix [Gentle, 1998]. On the other hand, as a Riemann sum, the approximation error of the discrete to the continuous Fourier transform decreases as the number of discrete points increases. This divergence might be the reason for the lower error we observe in FGP and merit further study in the future.

We demonstrate one generalization of the functional Gaussian process (FGP) to accommodate non-stationary or non-Gaussian data. The latent smooth process  $\boldsymbol{\mu}$  is used as the transformed mean of the weight process and facilitate the sampling of the multivariate truncated normal distribution; it also functions as a cluster parameter for easy selection of the most likely cluster for each data point. This generalized model provides a nice interpretation to large and heterogeneous spatial data. The other popular non-stationary model is the spatial random effect (SRE) [Cressie and Johannesson, 2008], which utilizes the setup of spatial basis functions on multiple resolutions and achieves dimension reduction through a smaller set of knots. Alternatively, the GFGP model focuses directly on the finest resolution, except each component has a boundary delimited by the Dirichlet process. Regardless of the difference, FGP is compatible with and can be integrated into the SRE model. As one potential extension, GFGP can be used to model the process on the knots, which is a lattice process. As a result, for GFGP one can remove the restriction of lattice location in the data; for SRE, one can use a large number of knots to achieve very high resolution.

In addition to the GFGP model we proposed, there are many other directions the FGP can be extended to. One possibility is to use FGP in multiscale data, where in each level one can assign the same or different types of stationary covariance. Since all the layers share the same set of eigenvectors, the eigenvalues of the marginal matrix are simply a sum of the ones from each layer. The other direction may involve dimension reduction not in observation  $N$  but in covariance space dimension  $d$ , similar to the work by Bhattacharya et al. [2014]. As many elements of spectral density are close to 0 in a correlated process, the dimension reduction may further facilitate the estimation and increase model parsimony.

# SUPPLEMENTARY MATERIAL

## 7.1 Spectral densities for three spatial-temporal models

After the Fourier transform, the spectral densities for the three models can be found:

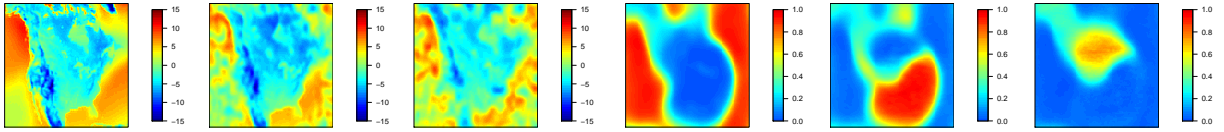
$$g_{\mathbb{M}(A)} = 2\pi\phi_1\rho_x\rho_y\exp\left(-\frac{\rho_x^2\omega_x^2}{2} - \frac{\rho_y^2\omega_y^2}{2}\right)\mathbf{1}_{t=1} + 2\phi_2\rho_t/(1 + \rho_t^2\omega_t^2)\mathbf{1}_{x=1,y=1}$$

$$g_{\mathbb{M}(S)} = 4\pi\phi\rho_x\rho_y\rho_t\exp\left(-\frac{\rho_x^2\omega_x^2}{2} - \frac{\rho_y^2\omega_y^2}{2}\right)/(1 + \rho_t^2\omega_t^2)$$

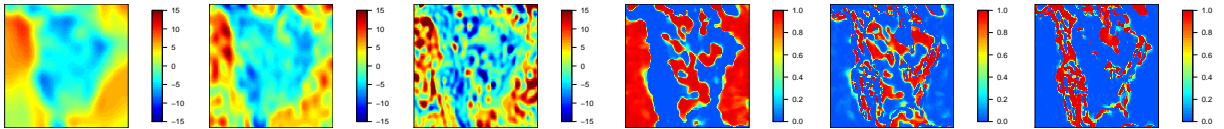
$$g_{\mathbb{M}(NS)} = 2\pi\phi\rho_x\rho_y \int_{\mathbb{R}} \exp(-it\omega_t)\exp\left(-\frac{\rho_x^2\omega_x^2}{2(1 + 2\rho_x^2|t|/c_1)} - \frac{\rho_y^2\omega_y^2}{2(1 + 2\rho_y^2|t|/c_2)} - \frac{|t|}{\rho_t}\right) / \sqrt{(1 + 2\rho_x^2|t|/c_1)(1 + 2\rho_y^2|t|/c_2)} dt$$

where  $g_{\mathbb{M}(NS)}$  does not have closed form for the last integration over  $t$ , but can be evaluated via fast Fourier transform rapidly.

## 7.2 Components in $\mathbb{M}(A)$ and $\mathbb{M}(S)$ and Parameter Estimates in $\mathbb{M}(NS)$



(a) Three components in model  $\mathbb{M}(A)$  in 1995 (b) Corresponding weights in model  $\mathbb{M}(A)$  in 1995



(c) Three components in model  $\mathbb{M}(S)$  in 1995 (d) Three components in model  $\mathbb{M}(S)$  in 1995

Figure 7: The 3 stationary components estimated by the GFGP in  $\mathbb{M}(A)$  and  $\mathbb{M}(S)$ . Due to the limited flexibility in  $\mathbb{M}(A)$ , its weight process cannot fit the data as well as the other two models.

	Component 1	Component 2	Component 3	Component 4
$\rho_x$ for $\boldsymbol{\mu}_{zl}$	12.17 (0.13)	4.11 (0.07)	8.26 (0.09)	8.47 (0.13)
$\rho_y$ for $\boldsymbol{\mu}_{zl}$	10.89 (0.08)	4.87 (0.07)	8.50 (0.08)	9.39 (0.19)
$\rho_t$ for $\boldsymbol{\mu}_{zl}$	16.43 (0.58)	45.61 (2.33)	29.04 (1.48)	23.07 (1.85)
$c_1$ for $\boldsymbol{\mu}_{zl}$	6347 (451)	61.72 (2.01)	2400 (145)	1738 (204)
$c_2$ for $\boldsymbol{\mu}_{zl}$	4615 (239)	73.38 (1.21)	2396 (146)	2083 (94)
$\phi$ for $\boldsymbol{\mu}_{zl}$	6.71 (0.39)	3.30 (0.07)	10.89 (0.71)	11.63 (0.56)
$\rho_x$ for $\boldsymbol{\mu}_{\nu l}$	4.19 (0.08)	37.29 (0.77)	1.32 (0.02)	4.44 (0.09)
$\rho_y$ for $\boldsymbol{\mu}_{\nu l}$	4.68 (0.07)	34.05 (0.54)	1.35 (0.01)	3.82 (0.05)
$\rho_t$ for $\boldsymbol{\mu}_{\nu l}$	$1.4 \times 10^5$ ( $3.1 \times 10^4$ )	22.87 (1.34)	$3.0 \times 10^6$ ( $2.2 \times 10^5$ )	$2.2 \times 10^6$ ( $6.0 \times 10^5$ )
$c_1$ for $\boldsymbol{\mu}_{\nu l}$	$1.6 \times 10^5$ ( $1.0 \times 10^4$ )	$2.1 \times 10^4$ ( $2.3 \times 10^3$ )	$4.5 \times 10^4$ ( $1.1 \times 10^3$ )	$8.0 \times 10^4$ ( $3.6 \times 10^3$ )
$c_2$ for $\boldsymbol{\mu}_{\nu l}$	$9.0 \times 10^4$ ( $1.3 \times 10^4$ )	$2.4 \times 10^4$ ( $1.9 \times 10^3$ )	$4.6 \times 10^4$ ( $1.7 \times 10^3$ )	$3.7 \times 10^4$ ( $9.5 \times 10^3$ )
$\phi$ for $\boldsymbol{\mu}_{\nu l}$	2.9 (0.14)	2.81 (0.15)	3.00 (0.13)	3.11 (0.12)
$\sigma^2$	1.82 (0.05)			
Frequency (%)	178481 (40%)	128379 (29%)	87923 (20%)	43397 (10%)

Table 4: The parameter estimates in model  $\mathbb{M}(NS)$ .

### 7.3 Posterior Sampling for Generalized Functional Gaussian Process

For effective computation we use latent variables  $\{\mathbf{M}, \mathbf{R}, \mathbf{Y}, \mathbf{U}\}$  in posterior sampling. We use  $M(s) = l$  to denote the event that  $Z_s = Z_l(s)$ . Equivalently,  $\mathbf{M}$  can be expressed as a series of stick-breaking event  $\mathbf{R}$ . We assume  $\mathbf{Y}_l \sim N(\boldsymbol{\mu}_{\nu l}, \mathbf{I})$  and  $U(s) \sim \text{Unif}(0, \omega_{M(s)})$ .

We iteratively sample from the posterior distributions:

1. Draw  $M(s)|U, Z(s), \boldsymbol{\mu}_{zl}(s)$  from  $l \in \{1, 2, \dots\}$  according to  $Pr(M(s) = l) \propto \mathbf{1}_{\omega_l > U(s)} Pr(Z(s)|\boldsymbol{\mu}_{zl}(s), \sigma_l^2)$ , for  $s = 1, 2, \dots, N$ .
2. Transform  $M(s)$  to  $R_l(s)$  and sample missing  $R_l(s) \sim \text{Bern}(\Phi(\boldsymbol{\mu}_{\nu l}(s)))$  for  $l = 1, 2, \dots$  and  $s = 1, 2, \dots, N$ .
3. Sample  $Y_l(s)|R_l(s), \boldsymbol{\mu}_{\nu l}(s)$  from  $N(\mu_l, 1)(\mathbf{1}_{Y_l(s) \geq 0, R_l(s)=1} + \mathbf{1}_{Y_l(s) < 0, R_l(s)=0})$ .
4. Update  $\boldsymbol{\theta}_{\nu l}$ , sample  $\boldsymbol{\mu}_{\nu l}|\mathbf{Y}_l$  as in (9), for  $l = 1, 2, \dots$  and update  $\boldsymbol{\nu}_l = \Phi(\boldsymbol{\mu}_{\nu l})$
5. Compute  $\boldsymbol{\omega}_l = \boldsymbol{\nu}_l \prod_{k < l} (1 - \boldsymbol{\nu}_k)$  and sample  $U(s) \sim \text{Unif}(0, \omega_{M(s)}(s))$
6. Update  $\boldsymbol{\theta}_{zl}$ , sample  $\boldsymbol{\mu}_{zl}|\mathbf{Z}_{lo}, \mathbf{Z}_{lm}$  and  $\mathbf{Z}_{lm}$  as in (9), for  $l = 1, 2, \dots$ ,

## References

- James H Albert and Siddhartha Chib. Bayesian analysis of binary and polychotomous response data. *Journal of the American Statistical Association*, 88(422):669–679, 1993.
- Ethan B Anderes and Michael L Stein. Local likelihood estimation for nonstationary random fields. *Journal of Multivariate Analysis*, 102(3):506–520, 2011.
- Sudipto Banerjee, Alan E Gelfand, and Bradley P Carlin. *Hierarchical modeling and analysis for spatial data*. CRC Press, 2004.
- Sudipto Banerjee, Alan E Gelfand, Andrew O Finley, and Huiyan Sang. Gaussian predictive process models for large spatial data sets. *Journal of the Royal Statistical Society: Series B (Statistical Methodology)*, 70(4):825–848, 2008.
- James O Berger, Victor De Oliveira, and Bruno Sansó. Objective Bayesian analysis of spatially correlated data. *Journal of the American Statistical Association*, 96(456):1361–1374, 2001.
- Anirban Bhattacharya, Debdeep Pati, and David Dunson. Anisotropic function estimation using multi-bandwidth Gaussian processes. *The Annals of Statistics*, 42(1):352–381, 2014.
- E Cheney and David Kincaid. *Numerical mathematics and computing*. Cengage Learning, 2012.
- Nidhan Choudhuri, Subhashis Ghosal, and Anindya Roy. Bayesian estimation of the spectral density of a time series. *Journal of the American Statistical Association*, 99(468):1050–1059, 2004.
- James W Cooley and John W Tukey. An algorithm for the machine calculation of complex fourier series. *Mathematics of computation*, 19(90):297–301, 1965.
- Noel Cressie and Hsin-Cheng Huang. Classes of nonseparable, spatio-temporal stationary covariance functions. *Journal of the American Statistical Association*, 94(448):1330–1339, 1999.

- Noel Cressie and Gardar Johannesson. Fixed rank kriging for very large spatial data sets. *Journal of the Royal Statistical Society: Series B (Statistical Methodology)*, 70(1):209–226, 2008.
- Noel Cressie, Tao Shi, and Emily L Kang. Fixed rank filtering for spatio-temporal data. *Journal of Computational and Graphical Statistics*, 19(3):724–745, 2010.
- Jason A Duan, Michele Guindani, and Alan E Gelfand. Generalized spatial Dirichlet process models. *Biometrika*, 94(4):809–825, 2007.
- Andrew O Finley, Sudipto Banerjee, and Bradley P Carlin. spbayes: an r package for univariate and multivariate hierarchical point-referenced spatial models. *Journal of Statistical Software*, 19(4):1, 2007.
- Montserrat Fuentes. Spectral methods for nonstationary spatial processes. *Biometrika*, 89(1):197–210, 2002.
- Montserrat Fuentes. Approximate likelihood for large irregularly spaced spatial data. *Journal of the American Statistical Association*, 102(477):321–331, 2007.
- Montserrat Fuentes and Richard L Smith. A new class of nonstationary spatial models. Technical report, Technical report, North Carolina State University, Raleigh, NC, 2001.
- Reinhard Furrer, Douglas Nychka, and Stephen Sain. fields: Tools for spatial data. *R package version*, 6(11), 2009.
- James E Gentle. *Numerical linear algebra for applications in statistics*. Springer, 1998.
- Tilmann Gneiting. Nonseparable, stationary covariance functions for space–time data. *Journal of the American Statistical Association*, 97(458):590–600, 2002.
- Robin Henderson, Peter Diggle, and Angela Dobson. Joint modelling of longitudinal measurements and event time data. *Biostatistics*, 1(4):465–480, 2000.
- David Higdon. A process-convolution approach to modelling temperatures in the north atlantic ocean. *Environmental and Ecological Statistics*, 5(2):173–190, 1998.

- IA Ibragimov. On estimation of the spectral function of a stationary Gaussian process. *Theory of Probability & Its Applications*, 8(4):366–401, 1963.
- Hemant Ishwaran and Lancelot F James. Gibbs sampling methods for stick-breaking priors. *Journal of the American Statistical Association*, 96(453), 2001.
- Neil D Lawrence and Michael I Jordan. Semi-supervised learning via Gaussian processes. In *Advances in neural information processing systems*, pages 753–760, 2004.
- Miguel Lázaro-Gredilla, Joaquin Quiñonero-Candela, Carl Edward Rasmussen, and Aníbal R Figueiras-Vidal. Sparse spectrum Gaussian process regression. *The Journal of Machine Learning Research*, 11:1865–1881, 2010.
- Jason L Loepky, Jerome Sacks, and William J Welch. Choosing the sample size of a computer experiment: A practical guide. *Technometrics*, 51(4), 2009.
- Steven N MacEachern. Dependent Dirichlet processes. *Unpublished manuscript, Department of Statistics, The Ohio State University*, 2000.
- LO Mearns, WJ Gutowski, R Jones, LY Leung, S McGinnis, AMB Nunes, and Y Qian. The North American regional climate change assessment program dataset. *National Center for atmospheric research earth system grid data portal, Boulder, CO. Data downloaded*, pages 01–03, 2011.
- Christopher J Paciorek and Mark J Schervish. Spatial modelling using a new class of nonstationary covariance functions. *Environmetrics*, 17(5):483–506, 2006.
- Jamis J Perrett. *A SAS/IML companion for linear models*. Springer, 2010.
- Alex J Smola and Bernhard Schölkopf. Sparse greedy matrix approximation for machine learning. 2000.
- Jonathan R Stroud, Michael L Stein, and Shaun Lysen. Bayesian and maximum likelihood estimation for Gaussian processes on an incomplete lattice. *arXiv preprint arXiv:1402.4281*, 2014.

Peter Whittle. The analysis of multiple stationary time series. *Journal of the Royal Statistical Society. Series B (Methodological)*, pages 125–139, 1953.

Christopher Williams and Matthias Seeger. Using the nystrom method to speed up kernel machines. In *Proceedings of the 14th Annual Conference on Neural Information Processing Systems*, number EPFL-CONF-161322, pages 682–688, 2001.